Nanotechnology, Science and Applications

Dovepress

open access to scientific and medical research

Open Access Full Text Article

ORIGINAL RESEARCH

Timing and Mechanisms of Nanodiamond Uptake in Colon Cancer Cells

Alina Sigaeva*, Runrun Li*, Jan Jelle van Laar, Leon Wierenga, Romana Schirhagl

Department of Biomaterials and Biotechnology, Groningen University, University Medical Center Groningen, Groningen, the Netherlands

*These authors contributed equally to this work

Correspondence: Romana Schirhagl, Email romana.schirhagl@gmail.com

Introduction: As nanodiamonds become more and more widely used for intracellular labelling and measurements, the task of delivering these nanoparticles inside cells becomes more and more important. Certain cell types easily take up nanodiamonds, while others require special procedures.

Methods: In previous research, we found that HT-29 cells (a colon cancer cell line), which are notoriously difficult in the context of nanodiamond internalization, show increased uptake rates, when pre-treated with trypsin- ethylenediaminetetraacetic acid (trypsin-EDTA). However, the uptake mechanism has not been studied before. This article focuses on a more detailed investigation of the reasons underlying this phenomenon. We start by identifying the timing of fluorescent nanodiamond (FND) uptake in trypsin-EDTA pre-treated cells. We then use a combination of chemical inhibitors and Immunocytochemistry to identify the main pathways employed by HT-29 cells in the internalization process.

Results and Discussion: We investigate how these pathways are affected by the trypsin-EDTA pre-treatment and conclude by offering possible explanations for this phenomenon. We found that nanodiamonds are internalized via different pathways. Clathrin-mediated endocytosis proves to be the dominating mechanism. Trypsin-EDTA treatment increases particle uptake and affects the uptake mechanism.

Keywords: nanodiamonds, cell uptake, cancer cells, HT29 cells, NV centers, imaging

Introduction

With the development of attractive applications of nanoparticles in the field of imaging, targeted drug delivery, theranostics, vaccines, and biosensors, the cellular uptake mechanism of nanoparticles has also received increasing attention in recent years.[1–4] Nanodiamonds (NDs) are one of the most promising carbon nanomaterials, exhibiting chemical inertness, good biocompatibility, and the potential for surface modification. Fluorescent nanodiamonds (FNDs) can emit stable and bright fluorescence without bleaching and blinking. This property allows for long-term observations of living cells and has already been utilized in the bioimaging field.[5] Moreover, the optical properties of FNDs can be modulated through temperature or magnetic fields.[6] As a result, FNDs can be used as a tool for biosensor applications.[7] However, for intracellular measurements, FNDs need to be internalized by the cells first. In order to better understand and control the fate of FNDs inside the cell, their uptake mechanism should be clarified.

In general, nanoparticles enter the cells by endocytosis.[8] It is an energy-dependent process and includes two categories: phagocytosis and pinocytosis. Phagocytosis occurs primarily in specialized cells to take up particles larger than 500 nm. This uptake mechanism is used by macrophages and neutrophils, which are specialized for clearing pathogens, apoptotic cells, or debris.[9] Pinocytosis occurs in almost all types of eukaryotes and includes four main pathways: macropinocytosis, clathrin-dependent endocytosis, caveolin-dependent endocytosis, clathrin- and caveolin-independent endocytosis (which, in turn, can be dynamin-dependent or dynamin-independent).[10] Our aim in this article is to determine the mechanism(s) by which FNDs enter HT29 cells.

Received: 27 March 2024
Accepted: 24 May 2024
Published: 25 July 2024

Macropinocytosis is an actin-driven process that enables the cells to nonspecifically ingest larger volumes of the surrounding liquid. This liquid might include particles that might be present in the solution. Macropinocytosis often happens in combination with other pathways.

Clathrin-dependent endocytosis is an uptake mechanism where the clathrin protein assembles into characteristic basket-like structures around the forming endosome. This way, clathrin facilitates the necessary curving and pinching of the membrane.[11] This process is receptor-mediated, and particles below 200 nm are generally thought to enter the cells via this pathway.[12]

Caveolin-dependent endocytosis is also a receptor-mediated process via flask-shaped or spherical pits (called caveolae) that are coated with the protein caveolin.[13] It has been shown that certain types of nanoparticles (like silver nanoparticles) are internalized via this pathway, if their size is 50 nm or smaller.[14] In another study, nanodiamonds, coated with D-α-tocopherol polyethylene glycol 1000 succinate, were internalized by Caco-2 colon cancer cells via this pathway, even though the complexes were relatively large (approximately 200 nm).[15]

Apart from the above-mentioned mechanisms, clathrin- and caveolin- independent endocytosis has been described. This process can be both dynamin-dependent and dynamin-independent. Dynamin is a small GTPase, which forms a ring around the neck of a budding endosome. This ring contracts, as dynamin hydrolyses GTP, bending the cell membrane further.

This process brings the lipid layers closer together, which ultimately results in membrane fusion and scission of the endosome from the cell surface. Clathrin- and caveolin-independent endocytosis is still poorly understood and is an entire family of distinct pathways.[10] The exact mechanism of nanoparticle internalization depends on the type of cells (cell lines) and physicochemical properties of nanoparticles including size, shape, and surface properties. Gilleron et al have reported that lipid nanoparticles with the size of 40 nm are transported to HeLa cells via macropinocytosis, whereas in NIH3T3 they were internalized by clathrin-mediated endocytosis.[16] Huang et al demonstrated that internalization of nanohydroxyapatite into the smooth muscle cells was shape-dependent. In their work, different morphology of the crystals led to either macropinocytosis or clathrin-mediated endocytosis.[17] Often, multiple uptake pathways are used by the cell in parallel to internalize nanoparticles.

Various pathways of endocytosis have been reported for NDs in different cell types. The summary of published work is given in Table 1. Generally, clathrin-mediated endocytosis seems to be the most observed pathway, but other internalization mechanisms have been observed as well. One of the most used approaches to studying endocytosis pathways is to incubate the cells with chemical inhibitors, which interfere with certain mechanisms. However, most of the available inhibitors interfere with more than one pathway,[18,19] which should be taken into account, when interpreting the experimental results. Some of the commonly used inhibitors, which were also employed in this study, are listed in Table 2. In this study, we examine the early stages of FND internalization by HT-29 cells. We have recently described a new method that utilized trypsin-EDTA pre-treatment to increase the number of particles internalized by HT-29 cells.[20] However, the mechanism and timing of FND uptake have not been further investigated. Figure 1 shows possible uptake mechanisms that are discussed in this article. We report on the timing of the FND uptake, the three-dimensional distribution of internalized particles in non-detached, undisturbed cells, as well as the possible mechanisms behind the FND uptake.

Materials and Methods

Cell Lines

HT-29 is a human colon adenocarcinoma cell line. As received HT-29 cells as well as GFP-EpCAM modified (provided by Prof. Giepmans and his group) HT-29 cells were used to study the FND uptake. The original cell lines were purchased from Sigma Aldrich. EpCAM is a transmembrane glycoprotein involved in the formation of tight junctions between the neighboring epithelial cells. In this study, this protein was fused with green fluorescent protein (GFP) to visualize the cell surface in the transfected cells. The cell culture method and growth environment are similar to those described in our previous work.[19] In short, cells were cultured in complete Dulbecco's Modified Eagle Medium - high glucose (DMEM-HG) medium containing 10% of fetal bovine serum (FBS, ScienCell, USA) and 100 U/mL penicillin, 100 µg/mL streptomycin (Life Technologies) at +37°C, 5% CO_2.

Table 1 Internalization Pathways Reported for Nanodiamonds in Different Types of Cells

Reference	Nanodiamond Size	Nanodiamond Shape and Surface Modifications	Cell Type	Uptake Pathways
Moscariello et al, 2019[21]	40–55 nm	Coated with cationic, PEGylated denatured human serum albumin	bEnd.3 (mouse brain endothelial cells)	Caveolin-mediated endocytosis, clathrin-mediated endocytosis
Turánek Knötigová et al, 2019[22]	100 nm	Carboxylated, flake-like	THP-1 (human monocytes)	Macropinocytosis, physical piercing of the membrane
Liu et al, 2018[15]	196 nm	Coated with D-α-tocopherol polyethylene glycol 1000 succinate, loaded with curcumin	Caco-2 (human colorectal adenocarcinoma)	Clathrin-mediated endocytosis, caveolin-mediated endocytosis, macropinocytosis
Solarska-Ściuk et al, 2014[23]	<20 nm	Functionalized with Trolox C	HUVEC-ST (human umbilical vein endothelial cells), A549 (human alveolar basal epithelial cells, adenocarcinomic)	A549: caveolin-mediated endocytosis, clathrin-mediated endocytosis HUVEC-ST: clathrin-, caveolin-, dynamin-independent endocytosis
Schrand et al, 2011[24]	4 nm; form aggregates of 150 nm	Functionalized with tetramethylrhodamine	N2A (mouse neuroblastoma)	Clathrin-mediated endocytosis
Faklaris et al, 2009[25]	46 nm	–	HeLa (human cervical cancer cells)	Clathrin-mediated endocytosis
Vaijayanthimala et al, 2009[26]	140 nm	Carboxylated; poly-L-lysine-coated	HeLa (human cervical cancer cells), 3T3-L1 (mouse pre-adipocytes)	Clathrin-mediated endocytosis
Liu et al, 2009[27]	100 nm	Carboxylated	3T3-L1 (mouse pre-adipocytes), A549 ((human alveolar basal epithelial cells, adenocarcinomic)	Macropinocytosis, clathrin-mediated endocytosis

Table 2 Chemical Inhibitors of Endocytosis

Inhibitor	Main Affected Pathway	Mechanism of Action	Cross-Interference with other Endocytic Pathways
Chlorpromazine	Clathrin-mediated endocytosis (CME)	Prevents the formation of clathrin coating on the surface of endocytic vesicles	Little to none
Genistein	Caveolin-mediated endocytosis (CavME)	Prevents the depolymerization of cortical actin, which is necessary for CavME	Interferes with dynamin recruitment, which can affect dynamin-dependent pathways (CME, clathrin- and caveolin-independent dynamin-dependent pathways)
Amiloride	Macropinocytosis	Inhibits Na^+/H^+ exchange at the membrane	Can disturb actin dynamics, which can affect the pinching of endocytic vesicles and subsequent transport of endosomes
Dynasore	All dynamin-dependent pathways, including CME and CavME	Inhibits activity of dynamin	Highly non-specific, inhibits a large group of uptake pathways
Cytochalasin D	Phagocytosis, macropinocytosis	Causes disassembly of actin filaments	Interferes with most endocytic pathways

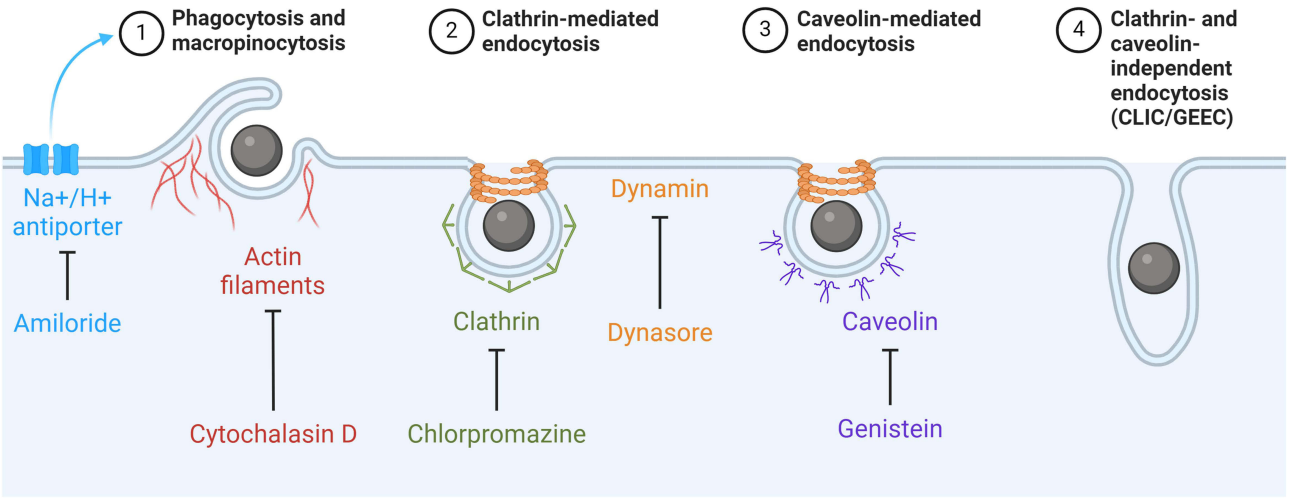

Figure 1 Common endocytic pathways. Coloured captions indicate important proteins involved in endocytosis, as well as the corresponding chemical inhibitors used in this study. Figure was created with BioRender.com.

Fluorescent Nanodiamonds

120-nanometer FNDs were purchased from Adamas Nanotechnologies. The particles contained around 1000 nitrogen-vacancy centers per particle and were obtained by grinding larger HPHT diamonds followed by irradiation and annealing. Due to an acid cleaning step at the end of fabrication, these particles are oxygen terminated. These particles have been characterised previously.[28,29] The concentration of FND stock suspension provided by the manufacturer is 1 mg/mL. For the FND internalization experiments, the stock solution was diluted in pure FBS. This step prevents aggregation and results in a small layer of FBS coating on the FND surface.[30] While the bare FNDs had a zeta potential of −22 mV and a hydrodynamic diameter of 120 nm, the FBS coating resulted in a zeta potential of −18 mV and a hydrodynamic diameter of 130 nm (determined by dynamic light scattering, Zetasizer (Malvern Panalytical)). Then, we added the serum-free DMEM-HG medium, to obtain a solution containing 10% FBS and 3 μg/mL of FNDs.

FND Internalization

HT-29 cells were seeded on 35-mm glass bottom Petri dishes and cultured to reach 70–90% confluency at +37°C, 5% CO_2. On the day of the experiment, the cells were exposed to the FND-containing medium, according to one of the two experimental protocols.

In the first case ("FNDs on top"), the cell culture medium was replaced with FND-containing DMEM-HG. The cells were incubated for a total of 2, 4, 6, or 8 hours. After 2 hours, the FND-containing medium was replaced with FND-free DMEM-HG.

In the second case, HT-29 cells were briefly rinsed with trypsin-EDTA, which has been previously shown to improve FND internalization in this cell line. The trypsin-EDTA pre-treatment was performed for 30 seconds in an incubator. We controlled the cell morphology with a bright-field microscope. We observed cells rounding and detaching from each other but remaining attached to the bottom of the dish. Afterwards, the cells were incubated with FND-containing medium for (2+0), (2+2), (2+4), or (2+6) hours, as described above. At the end of the incubation, the cells were rinsed with phosphate-buffered saline (PBS) and fixed with 3.7% paraformaldehyde for 12 minutes for the microscopic analysis.

Inhibition of FND Uptake

GFP-EpCAM HT-29 cells were cultured in glass bottom Petri dishes, as described previously. To assess the FND internalization pathway, the cells were pretreated with five different inhibitors for 30 minutes at 37°C. The inhibitors had the following concentrations: genistein 200 μM, dynasore 80 μM, cytochalasin D 0.5 μg/mL, chlorpromazine 10 μg/mL, and amiloride 200 μM. After the pre-incubation, the cells were exposed to the FND-containing medium, as described in

FND Internalization. In each case, the medium was supplemented with the respective inhibitor. The incubation with FNDs lasted for (2+4) hours.

In addition, we performed another set of uptake inhibition experiments at +4 °C, which depletes the cells of energy and blocks all active transport pathways. In this case, the procedure was identical to that described in FND Internalization, but all the solutions were cold, and the cells were incubated with the FNDs in the fridge.

Cell Viability Assays

We determined whether the five inhibitors and +4 °C treatment would affect the metabolic activity of the cells. To this end we used a 3-(4,5-dimethylthiazol-2-yl)-2,5-diphenyltetrazolium bromide (MTT) assay that has been described elsewhere.[31–33] For the assay, HT-29 cells were seeded in 96-well plates and cultured for 24 h. Then, the cells were exposed to the inhibitors and the FND-containing medium, as described in Inhibition of FND Uptake. Additionally, we had HT-29 cells treated with FND-free medium, as the control for the impact of nanodiamond uptake on the cell metabolic activity. When the incubation was over, the medium was replaced with 100 µL of MTT solution in PBS per well. The MTT concentration was 5 mg/mL. The cells were incubated with MTT for 2 h at +37 °C, and the formation of dark-purple formazan crystals inside the cytoplasm was confirmed with bright-field microscopy. The formazan crystals form due to the activity of intracellular reductases, which reflects the level of cell metabolism. After removing the MTT solution we added 100 µL of DMSO to dissolve the formazan crystals for 15 min. The absorbance of the solution was measured at 560 nm using a microplate reader.

Immunocytochemistry

In order to better understand the intracellular fate of FNDs, we performed immunostaining of the fixed HT-29 cells (GFP-free) for certain marker proteins of different endocytic pathways. For these experiments, the cells were fixed after either (2+0) or (2+4) hours of incubation. The proteins of interest included EEA1 (marker of early endosomes; Abcam, ab109110), LAMP-1 (marker of lysosomes and endolysosomes; ThermoFisher Scientific, # 53-1079-42), clathrin (marker of clathrin-mediated endocytosis; ThermoFisher Scientific, # MA1-065-A488), caveolin (marker of caveolin-mediated endocytosis; ThermoFisher Scientific, # PA5-17447), and Rab34 (marker of macropinocytosis; Abcam, ab73383). For unconjugated antibodies, a respective secondary antibody, conjugated with FITC, was used: donkey-anti-rabbit IgG (Jackson, 711-095-152) or goat-anti-mouse IgG (Jackson, 115-095-146).

The fixed cells were washed three times with PBS, 5 minutes per wash. Then the cells were permeabilized with 0.1% Triton-X100 for 15 minutes, followed by 3×5 minutes of washing with PBS. The samples were incubated with 1% bovine serum albumin in PBS (PBSA) to block the sites of non-specific binding for 30 minutes. Then cells were stained with primary antibodies in PBSA at the concentrations recommended by the manufacturer over night at +4°C. The next day, the samples were washed three times with PBSA, 5 minutes per wash, and incubated with secondary antibodies in PBSA over night at +4°C in the dark. Afterwards, the samples were washed with PBSA and PBS to remove the non-bound antibodies, and stored in 1% paraformaldehyde solution in PBS at +4°C until the imaging.

Cell Imaging, Image Processing and Analysis

Z-stack images of the cells were taken with a Zeiss LSM780 confocal microscope. The full z-stack slices of cells were obtained and all fluorescent signals (GFP, FND, FITC) were collected with a cubic voxel of 132 × 132×132 nm. The images were processed and analyzed, as described in our previous study.[19] Briefly, z-stack images were first deconvolved with FIJI, using "Diffraction PSF 3D" and "Iterative Deconvolve 3D" plugins. Then all particles in the volume of the z-stacks were detected, using the "3D Objects Counter" plugin. The particles inside the cells and on the cell membrane were included in the analysis, while excluding those outside the cell membrane, based on the GFP signal or the bright-field images.

For GFP-EpCAM-expressing cells, the deconvolved images of the GFP channel were transformed to a 3D Euclidean Distance Map of cells, where we obtained the minimal distance between the particle and the cell membrane. The number of internalized FNDs was also acquired for each analysed cell. Moreover, the height of each cell was determined, and the relative vertical position of each internalized particle was derived from that (0% meaning FNDs at the bottom of the cell, 100% - at the top of the cell). These locations were analysed to better understand where particles end up in addition to the uptake mechanism which was described earlier.

For the cells after immunostaining, we calculated the proportion of FNDs colocalizing with the signal from the protein of interest. A particle was considered colocalized, if the minimal distance between the particle and the structure of interest was equal to 0. This analysis was performed on a z-stack basis.

Statistical Analysis

The results were analyzed, using a one-way ANOVA, followed by a Kruskall-Wallis test for multiple comparisons, or using the Mann–Whitney test, if only two groups had to be compared. All statistical analysis was performed in GraphPad 9.3. Statistical significance of the differences is reported as follows: "ns" for $p > 0.05$, "*" for $p < 0.05$, "**" for $p < 0.01$, "***" for $p < 0.001$, "****" for $p < 0.0001$.

Results

Early Effects of Trypsin-EDTA Treatment on the FND Uptake and Intracellular Distribution

As expected, pre-treating the cells with trypsin-EDTA Results in higher uptake rates already within the first two hours of incubation (Figure 2). As the (2+4) incubation scheme leads to the highest FND counts in both groups, we used it for the experiments on the uptake inhibition to increase the sample size.

The intracellular distribution of FNDs is shown in Figure 3. The distance of internalized FNDs from the cell membrane and their vertical distribution changed slightly, but the median value did not change significantly. Both non-treated and trypsin-EDTA pre-treated cells show a similar distribution of FNDs in the endolysosomal compartment. As expected, the proportion of FNDs in the (endo)lysosomes increases with longer incubation time. Trypsin-EDTA pre-treatment does not seem to affect the general progression of FNDs from early to late endosomes.

Influence of the Endocytosis Inhibitors on the Cell Metabolic Activity

The effects of chlorpromazine, dynasore, amiloride, cytochalasin D, genistein, and +4°C-incubation on the metabolic activity of HT-29 cells were investigated before studying the mechanism of diamond endocytosis. The results of the six experimental groups showed that the cellular metabolic activity was distributed around ±20% of the control group, which is within the range of normal variation (Figure 4). Trypsin-EDTA pre-treatment, combined with +4°C-incubation, resulted in a decrease in metabolic activity. As trypsin-EDTA forces the cells to detach from each other and from the bottom of the Petri dish, the cells need to re-establish those contacts. This is an active, energy-dependent process, which might be impeded by low temperature, causing cell stress. Moreover, if the cells fail to attach to the bottom of the dish,

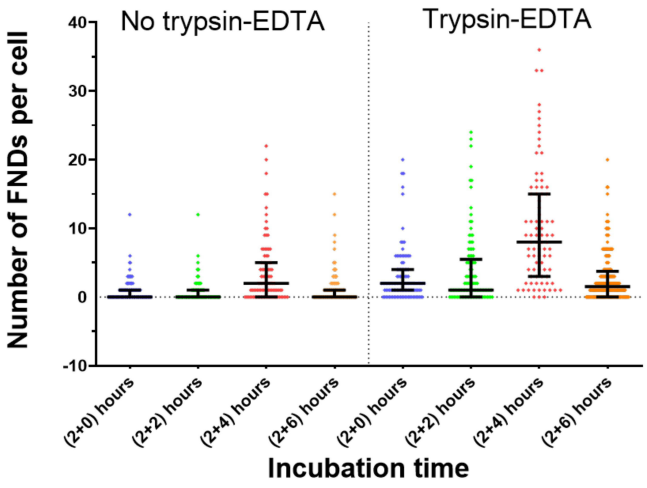

Figure 2 Number of FNDs detected inside the cells after different incubation times. The FNDs were counted in the confocal z-stacks, as described in Cell Imaging, Figure Processing and Analysis. The objects consisting of at least 8 voxels were considered FNDs. The lines in the plot show the median value, the error bars represent the interquartile range.

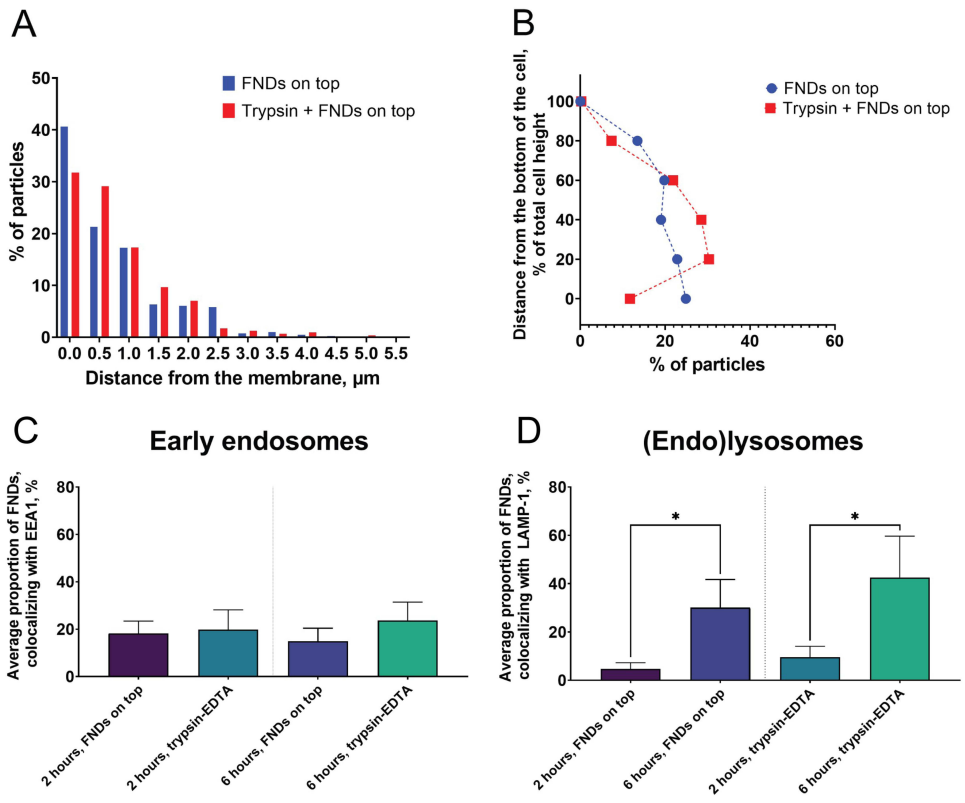

Figure 3 Intracellular distributions of FNDs in the control cells and in the cells, pre-treated with trypsin-EDTA. (**A** and **B**) At the (2+4) hours incubation time point, the distributions of FNDs inside the cells are slightly altered in case of trypsin-EDTA pre-treatment. The median values, however, do not change significantly. If the cells are pre-treated with trypsin-EDTA, more FNDs can be found further away from the cell membrane and closer to the middle part of the cell, as opposed to apical and basal parts. (**C** and **D**) Trypsin-EDTA pre-treatment does not affect the general progression of internalized FNDs from early to late endosomal compartments. Both at (2+0) and (2+4) hours of incubation, approximately 20% of FNDs colocalize with early endosome antigen 1 (EEA1), the marker of early endosomes. The proportion of FNDs colocalizing with Lysosomal Associated Membrane Protein 1 (LAMP-1), the protein associated with lysosomes and endolysosomes, increases with longer incubation times. Statistical differences are denoted by *p ≤ 0.05.

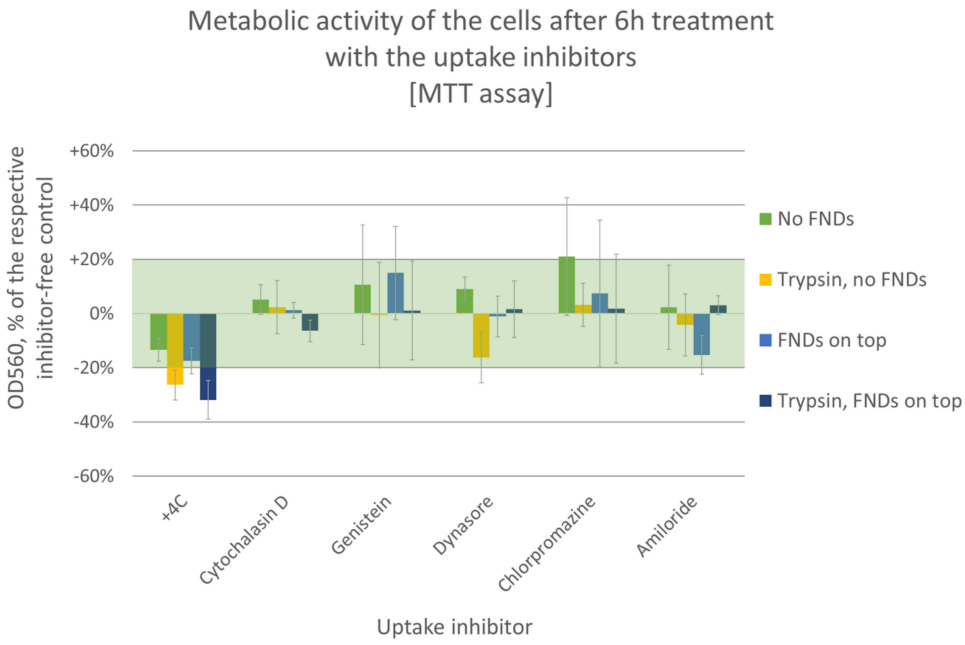

Figure 4 Changes in metabolic activity of HT-29 cells after the exposure to different endocytosis inhibitors, as reported by MTT assays. The physiological variation in metabolic activity (±20% of control) is shaded. The columns correspond to the average of 5 measurements, the error bars show standard deviations.

they can be washed away during the change of the medium. This would decrease the number of cells in the sample and the perceived metabolic activity of the cell population.

FNDs are Internalized via an Active Uptake Mechanism

In investigating the endocytic pathway in HT-29 cells, we used the low temperature to non-specifically inhibit active uptake pathways. Figure 5 shows that the FND uptake is significantly inhibited, when the cells are kept at +4°C. Representative images are shown in Figure 5 A and B and a quantification in Figure 5 C. This suggests that internalization of FNDs is an active transport process involving energy expenditure. Interestingly, FND uptake was still present in the "FNDs on top" protocol, which can either result from passive internalization of FNDs (eg, via direct membrane piercing) or be an artifact, as the depletion of the cell's energy reserves is not immediate, and some uptake might still take place during the early stages of the incubation. As the "FNDs on top" protocol generally yields rather low particle counts, it is more difficult to notice the inhibition of the uptake.

The particles that were internalized by the cells were found further away from the membrane, as compared to the FNDs internalized by the cells at +37°C (see Figure 6). This supports the hypothesis that the uptake observed in cold-treated cells is an artifact, the residual FNDs that were internalized during the early stages of the incubation and transported into the cytoplasm. Interestingly, in both non-treated and trypsin-EDTA pre-treated cells, FNDs were found to be closer to the basal part of the cell.

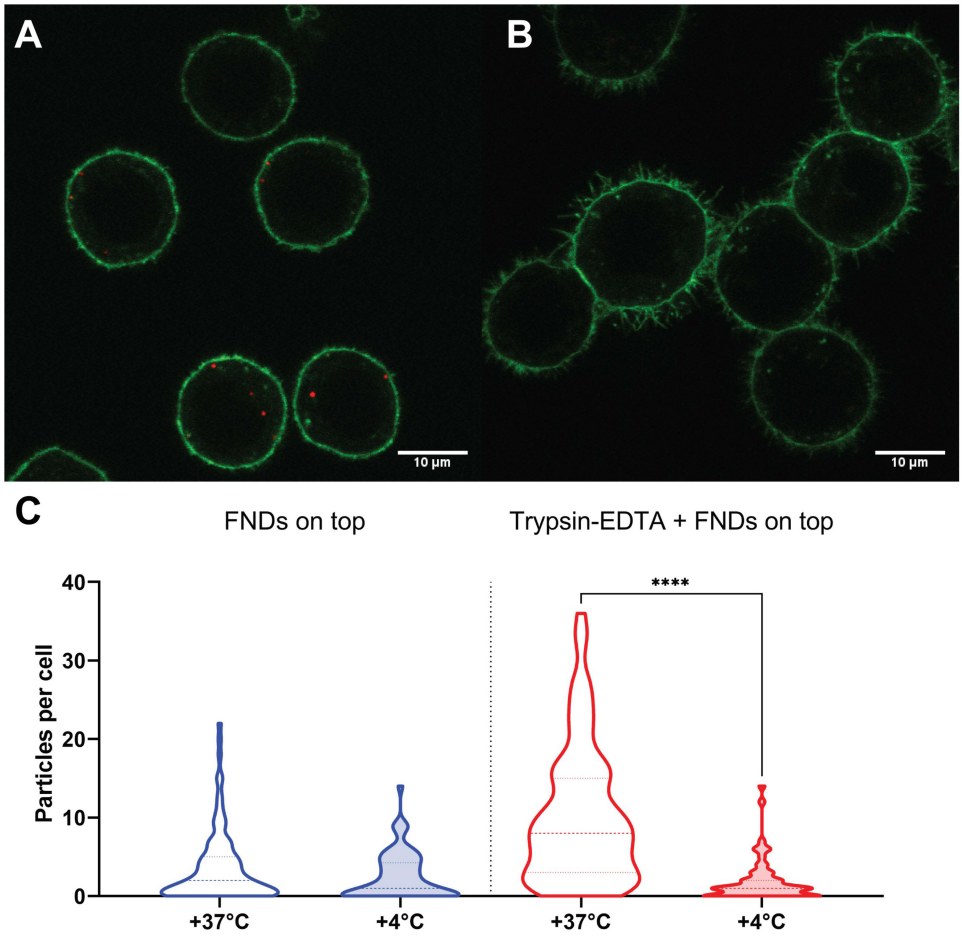

Figure 5 The effects of incubation at +4°C. (**A**) Trypsin-EDTA pre-treated HT-29 GFP-EpCAM cells after (2+4) hours of incubation with FNDs at +37°C. (**B**) Trypsin-EDTA pre-treated HT-29 GFP-Epithelial cell adhesion molecule (EpCAM) cells after (2+4) hours of incubation with FNDs at +4C. No FNDs can be found inside the cells. Notably, cells show a lot of protrusions of the cell membrane. Green – GFP-EpCAM, red – FNDs. (**C**) Number of internalized FNDs per cell. Statistical differences are denoted by ****$p \leq 0.0001$.

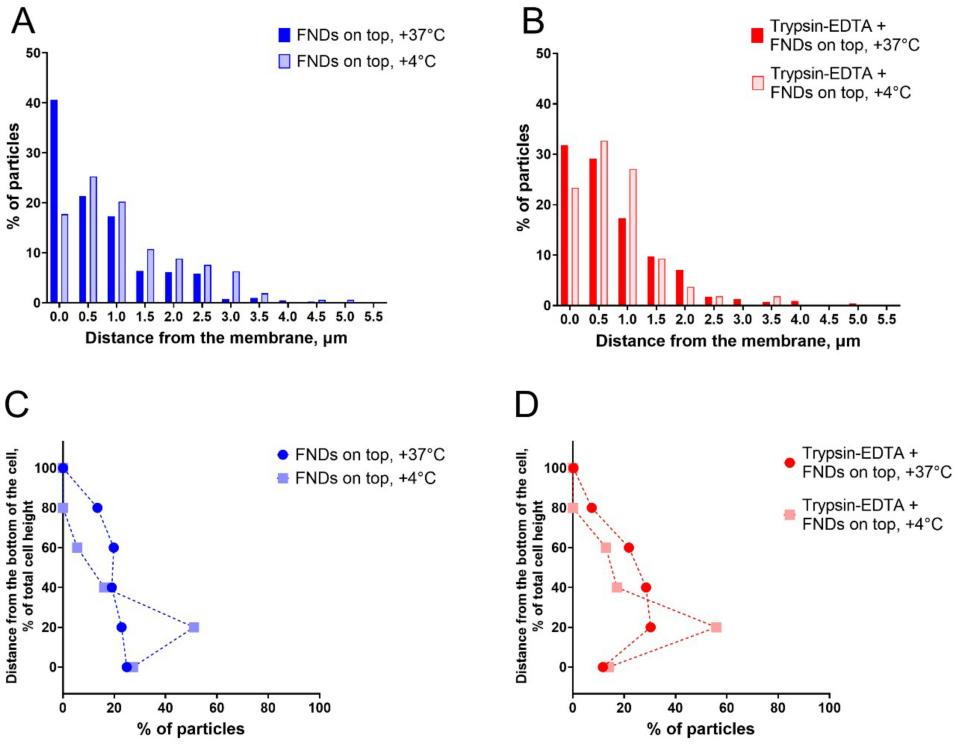

Figure 6 Intracellular distributions of internalized FNDs. (**A**) When the cells are incubated with FNDs at +37°C, most of the particles are found at the cell membrane. In case of +4°C incubation, the peak of the nanoparticle distribution shifts further away from the membrane. (**B**) Similarly, pre-treatment with trypsin-EDTA results in a distribution with the maximum close to the cell membrane. However, a larger portion of FNDs (approximately 70%, as opposed to 60% in panel (**A**) are located at least 0.5 µm away from the membrane. When the cells were incubated at +4°C, the maximum of the distribution shifts to a rate similar to non-treated cells. (**C** and **D**) Both in non-treated and trypsin-EDTA pre-treated cells, low temperature incubation leads to a larger portion of FNDs located in the basal part of the cell.

FND Uptake in HT-29 Cells Occurs Through a Combination of Endocytic Pathways

To further elucidate the uptake mechanism, cells were incubated with chlorpromazine, dynasore, amiloride, cytochalasin D, and genistein. The numbers of internalized FNDs per cell are summarized in Figure 7. All five inhibitors significantly lowered the FND counts, indicating that FNDs are internalized via a combination of pathways. Dynasore and amiloride treatment lead to significant differences between the "FNDs on top" and "trypsin-EDTA + FNDs on top" groups, affecting the pre-treated cells less than the non-treated ones. This might indicate that trypsin-EDTA pre-treated cells change the repertoire of endocytic pathways. We further investigated the effects of each of the inhibitors to get more insight on the mechanisms of the FND uptake.

Clathrin-Mediated Endocytosis is the Dominant FND Internalization Pathway in HT-29 Cells

HT-29 cells were found to contain many clathrin-positive vesicles, and those colocalize with a substantial portion of FNDs (Figure 8A). Surprisingly, in trypsin-EDTA pre-treated cells, significantly more particles were found to be associated with these vesicles (Figure 8B). As expected, chlorpromazine, the inhibitor of clathrin-mediated endocytosis, drastically reduced the number of internalized particles (Figure 8C).

In non-pre-treated cells, incubation with chlorpromazine resulted in a larger portion of FNDs colocalizing with the cell membrane (Figure 9A). In trypsin-EDTA pre-treated cells, chlorpromazine also caused FND retention at the membrane (Figure 9B). Additionally, the particles were mostly found in the basal part of the cell, which suggests that the clathrin-mediated uptake largely takes place from the apical part (Figure 9C). Trypsin EDTA pretreatment had no effect on the vertical distribution of the particles (Figure 9D).

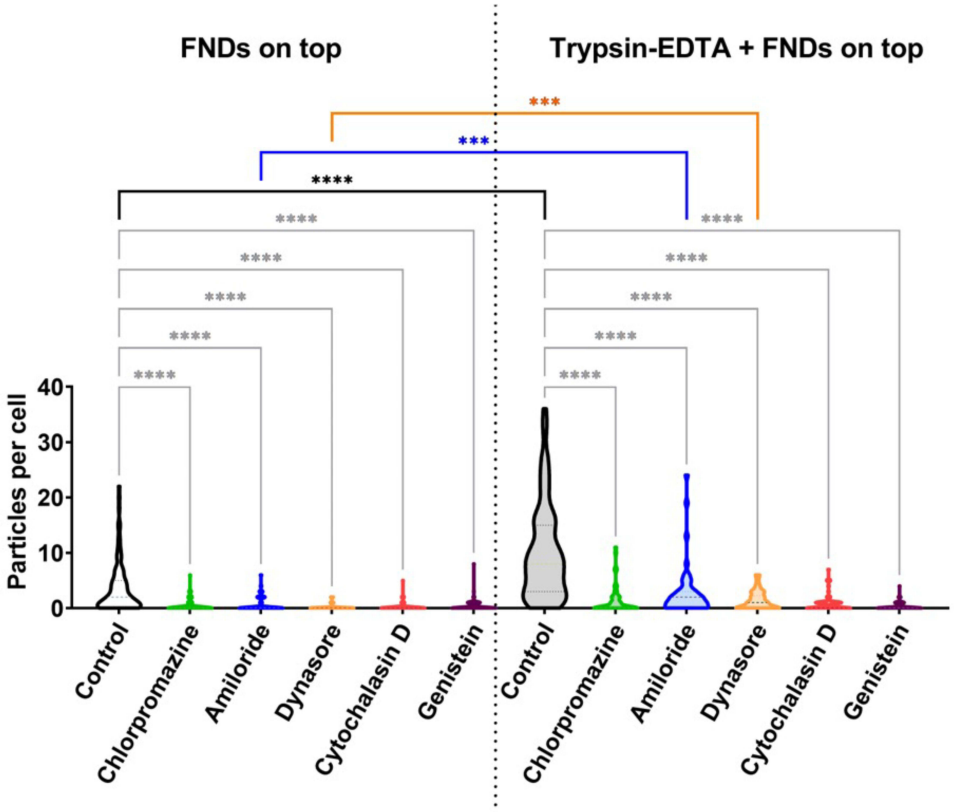

Figure 7 Number of FNDs, internalized by HT-29 cells after (2+4) hours of incubation in presence of the chemical inhibitors of endocytosis. Gray lines and asterisks show the statistical significance of the differences between the control cells (no inhibitor) and each of the inhibitor groups within one experimental protocol (either "FNDs on top" or "Trypsin-EDTA + FNDs on top"). Coloured lines and asterisks compare the same inhibitor between two experimental protocols (black – no inhibitor; blue – amiloride; Orange – dynasore). Statistical differences are denoted by ***p ≤ 0.001 and ****p ≤ 0.0001.

Caveolae-Mediated Endocytosis Plays a Smaller, Yet Significant Role in FND Uptake

Approximately 10–15% of FNDs colocalized with caveolin, both in non-treated and trypsin-EDTA pre-treated cells. There were no differences between the two groups, and genistein, the inhibitor of caveolin-mediated endocytosis, had a similar effect in both cases (see Figure 10). Genistein had a rather mild effect on the distance between the internalized particles and the cell membrane, but drastically affected the vertical distribution of FNDs. In non-trypsin-EDTA-treated cells, genistein resulted in a larger portion of the particles present in the apical part of the cell, the effect opposite to that of chlorpromazine. In trypsin-EDTA pre-treated cells, however, FNDs were accumulated in the basal part, and the uptake was reduced in the middle 40–60% of the cell (Figure 11).

Amiloride Affects the Uptake and Intracellular Distribution of FNDs to a Larger Degree in HT-29 Cells That Have Not Been Pre-Treated with Trypsin-EDTA

As shown in Figure 12, Amiloride, which is generally considered to interfere with macropinocytosis and phagocytosis, inhibits the uptake of FNDs in both trypsin-EDTA pre-treated and non-treated HT-29 cells. Surprisingly, almost none of the FNDs were found to be colocalized with macropinosomes, as visualized by Rab34. However, amiloride is known to interfere with actin dynamics,[34,35] and actin polymerization and depolymerization are vital for a range of endocytosis pathways. Therefore, the observed decrease in FND uptake might be an effect this interference with other pathways.

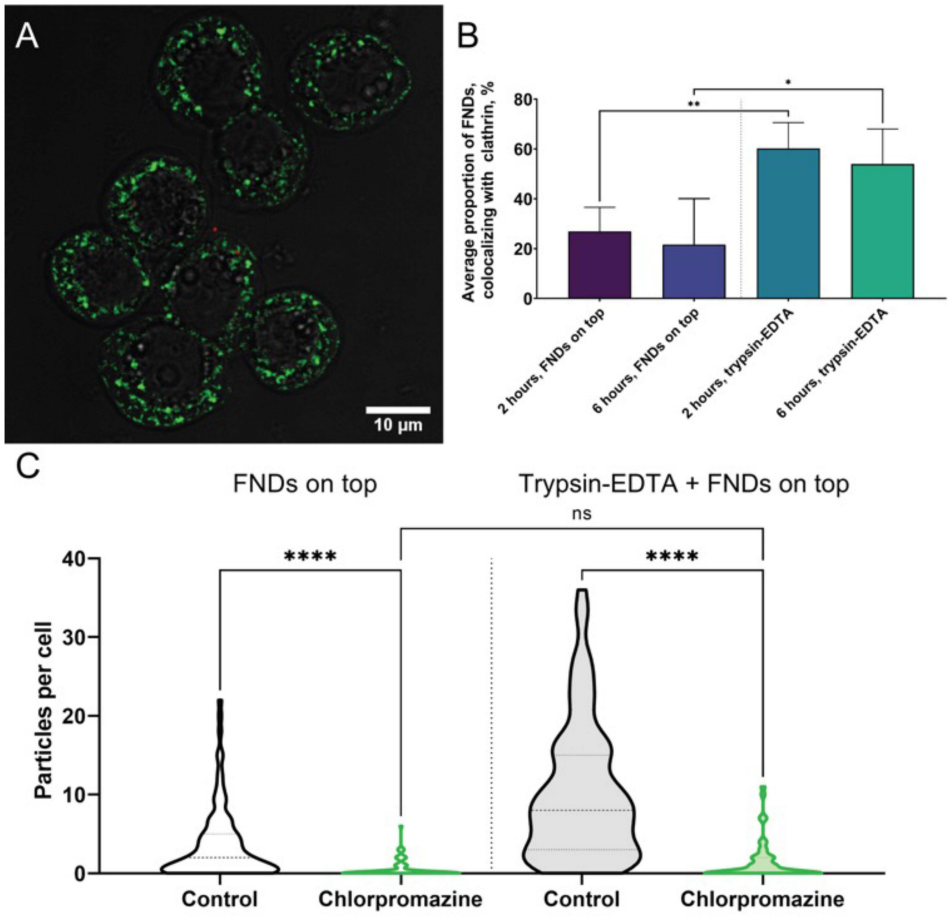

Figure 8 (**A**) HT-29 cells contain many clathrin-positive vesicles. Green – clathrin, red – FNDs. (**B**) In trypsin-EDTA pre-treated cells, a significantly larger portion of FNDs colocalizes with clathrin, both at (2+0) and (2+4) hours of incubation. (**C**) Chlorpromazine, the inhibitor of clathrin-mediated endocytosis, significantly reduces the number of internalized FNDs in both control and trypsin-EDTA pre-treated cells. Statistical significance of differences between the two control groups is not shown. Statistical differences are denoted by ns=not significant, *p ≤ 0.05, **p ≤0.01 and ****p ≤ 0.0001.

Cytochalasin D Reduces the FND Uptake in Both Non-Treated and Trypsin-EDTA Pre-Treated Cells

Cytochalasin D, which causes depolymerization of fibrillar actin, also has a pronounced effect on the number of internalized FNDs (Figure 13). Interestingly, the impact of amiloride on the distance between the particles and the cell membrane (Figure 14A and B) seems to be inverse to that of cytochalasin D (Figure 15A and B). Amiloride causes FND retention on the membrane in non-treated cells, while cytochalasin D affects trypsin-EDTA pre-treated cells. The impact on the vertical distribution (for amiloride in Figure 14C and D and for cytochalasin D in Figure 15C and D), however, is similar for those two inhibitors – they seem to affect the same area of the cell.

The Impact of Dynasore Resembles the Effects of Chlorpromazine on the FND Uptake and Distribution

As shown in Figure 16, dynasore generally reduces the number of internalized FNDs in both trypsin-EDTA-treated- and non-treated cells. Similarly to the chlorpromazine-treated groups (Figure 9A and B), dynasore-treated cells contain a larger portion of FNDs close to the cell membrane (Figure 17A and B). Interestingly, the vertical distribution of the internalized particles is also affected, but these changes are far more pronounced in control cells, as opposed to the trypsin-EDTA-treated cells (Figure 17C and D). Again, it resembles the effects of chlorpromazine on the vertical

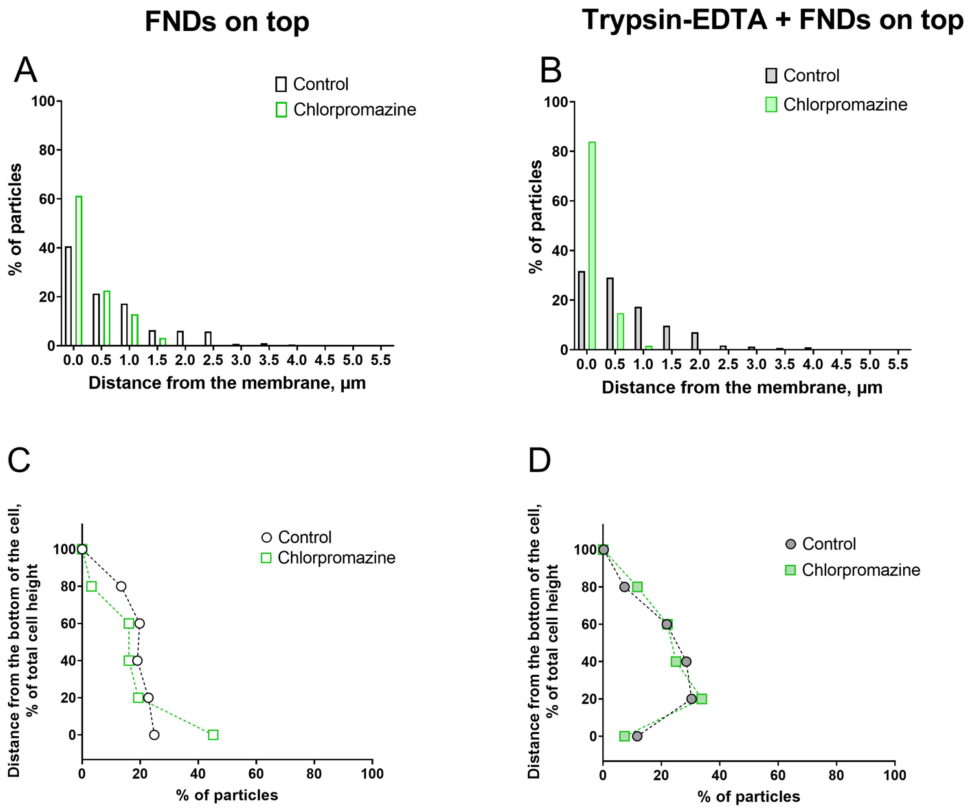

Figure 9 Intracellular distribution of internalized FNDs after (2+4) hours of incubation. Both in control and trypsin-EDTA-treated cells, chlorpromazine increases the proportion of particles at the cell membrane (**A** and **B**). It also affects the vertical distribution of internalized FNDs in control cells (**C**), but not in trypsin-EDTA-treated cells (**D**). In the control group ("FNDs on top"), chlorpromazine treatment results in more FNDs in the basal part and less FNDs in the apical part of the cells.

distribution of FNDs (Figure 9C and D). As dynasore is involved in pinching of the endosomes off the cell membrane, and clathrin-mediated endocytosis is the dominant internalization pathway, it is not surprising that these two inhibitors have a similar effect on the FND distribution in the cells.

Discussion

We demonstrate that the FND internalization rates increase already within the first 2 hours after trypsin-EDTA treatment. After these first two hours the medium is replaced by medium that does not contain FNDs. However, the number of internalised FNDs still increases until the 2+4 hour group. This is probably due to particles that are on the surface at the 2 hour time point but are ingested. After that, the particle number per cell decreases which can be attributed to excretion or cell division. Trypsin-EDTA treatment has been previously shown to improve the uptake of FNDs in HT-29 cells, however the details of this process were not clear. This treatment does not have a major effect on the distance between the FNDs and the cell membrane (ie, on the intracellular transport of FNDs away from the cell surface). However, it somewhat changes the vertical distribution of the particles inside the cell. We observe slightly more FNDs in the middle and basal part of the cell (20–40% of total cell height). This can be explained by the changes in either the particles' intracellular transport or in their entry point into the cell.

EDTA sequesters the Ca^{2+} ions, which are necessary for the interaction of cell adhesion molecules and for the cells forming tight junctions – highly impermeable connections located in the middle part of the cells. Trypsin cleaves the proteins from the cell membrane, further preventing the cells from being connected to each other. Intercellular junctions are important to maintain the apical-basal polarity of epithelial cells and to form a barrier, which makes the basal membrane of the cells virtually inaccessible for the material (fluids, molecules, particles) coming from above. The differences in basal and apical uptake of epithelial cells have been previously

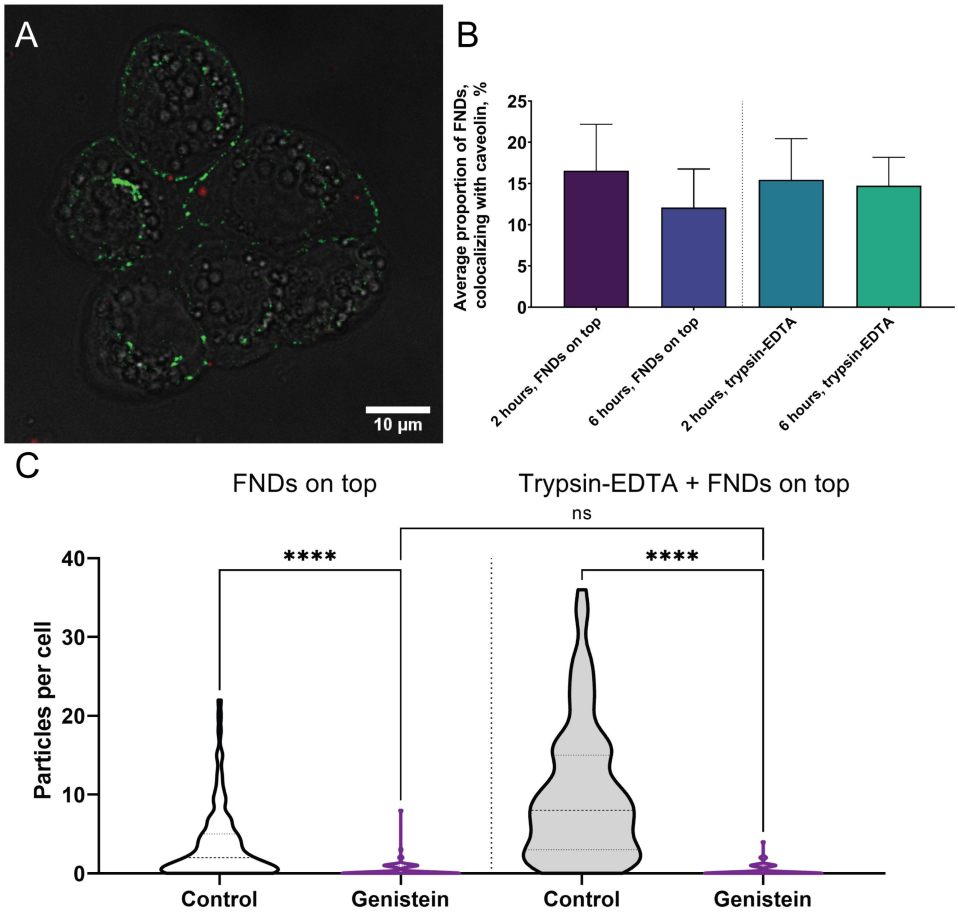

Figure 10 (**A**) Caveolae can be seen in HT-29 cells as punctate patterns on the cell membrane. Green – caveolin, red – FNDs. (**B**) Both in non-treated and trypsin-EDTA-treated cells, 10–15% of FNDs colocalize with caveolin at (2+0) and (2+4) hours of incubation. (**C**) Number of internalized FNDs after (2+4) hours of incubation in presence of genistein, the inhibitor of caveolin-mediated endocytosis. Statistical significance of differences between the two control groups is not shown. Statistical differences are denoted by ns=not significant and ****p ≤ 0.0001.

described.[10] Similarly, removing those differences by disturbing the cell-cell contacts has been proven to increase the uptake of lipoplex internalization in the cells that are generally difficult to transfect.[36]

Disruption of the tight junctions will inevitably increase the surface of the cell membrane available for FND binding and internalization. However, it might also affect the distribution of the receptors and multi-protein structures that are responsible for the uptake. To assess these processes, we investigated the vertical distribution of FNDs (assuming that it is influenced by the point of entry of the particles) and the way it is affected by the inhibitors of different endocytic pathways. These findings are summarized in Table 3.

The first pathway we analyzed was clathrin-mediated endocytosis. In epithelial cells (and HT-29 cells are of epithelial origin), there are two distinct populations of clathrin-coated pits: the apical and the basal ones. If the tight junctions are disrupted, the basal population will become available for the FND uptake, and the proportion of particles internalized via this way will increase. This is what we see in Figure 8B: trypsin-EDTA pre-treated cells contain a 2–3 times higher percentage of FNDs that colocalize with clathrin-coated vesicles. In non-treated cells, FNDs coming from the top would be mostly internalized via the apical pits. If the cells are treated with chlorpromazine, the inhibitor of this process, we would expect to see a decrease in the number of FNDs in the upper part of the cell. However, in trypsin-EDTA pre-treated cells, FNDs would be taken up over the entirety of the cell surface – hence, chlorpromazine would decrease the number of internalized particles equally at all heights, and

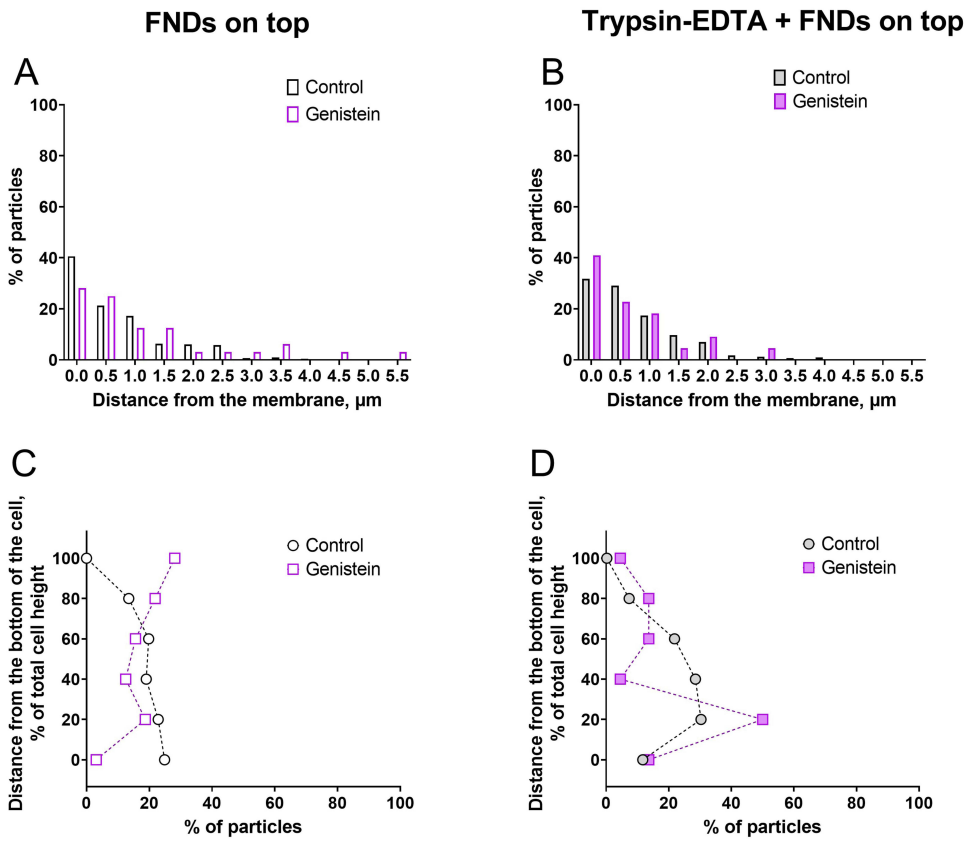

Figure 11 Intracellular distribution of internalized FNDs after (2+4) hours of incubation in presence of genistein. (**A**) Genistein does not increase the proportion of FNDs at the cell membrane in the non-trypsin-EDTA-pre-treated cells, but mildly impedes the progression of FNDs away from the cell periphery in trypsin-EDTA-treated cells (**B**). The impact of genistein on the vertical distribution of FNDs also differs between trypsin-EDTA-treated and non-treated cells. (**C**) In non-treated cells, genistein causes accumulation of FNDs in the apical region of the cells. (**D**) In contrast, cells, pre-treated with trypsin-EDTA, have a larger portion of FNDs located in the basal part.

the proportions in the vertical distribution would not change. Figure 8C as well as Table 3, show exactly such a response.

Another pathway we explored was caveolin-mediated endocytosis. Caveolae in epithelial cells are mostly found in the basal part of the cell, and this would be the population affected by genistein, the inhibitor of caveolin-mediated uptake. In non-trypsin-EDTA-treated cells, we see that genistein decreases the proportion of FNDs present in the basal part of the cell (Table 3). However, in trypsin-EDTA pre-treated cells, genistein mostly affects the middle population of the particles. This might stem from the redistribution of caveolae on the cell membrane, caused by the disruption of tight junctions and partial loss of apical-basal polarity. It is worth noting that the proportion of FNDs colocalizing with caveolin remains the same in both experimental groups – in contrast to previously discussed clathrin-mediated endocytosis. Trypsin-EDTA treatment thus does not seem to increase the probability of FNDs binding to the caveolae, only the location on the cell membrane, where this process occurs. Caveolae-mediated endocytosis seems to occur even in non-treated cells – possibly at the periphery of the cell clusters. If it is a relatively minor pathway of FND uptake, the added portion of available caveolae might be not large enough to affect the results. More thorough analysis of the distribution of caveolae, as well as the differences in FND uptake on the periphery of cell clusters, where more of the cell surface is available to the particles, and in the central part of the clusters, could shed more light on this process.

While macropinosomes were clearly seen in HT-29 cell, FNDs did not seem to colocalize with those vesicles. At the same time, amiloride treatment substantially decreased the number of internalized particles. This discrepancy emphasizes the need for using complementary techniques to analyze the endocytic pathways. Amiloride is known to

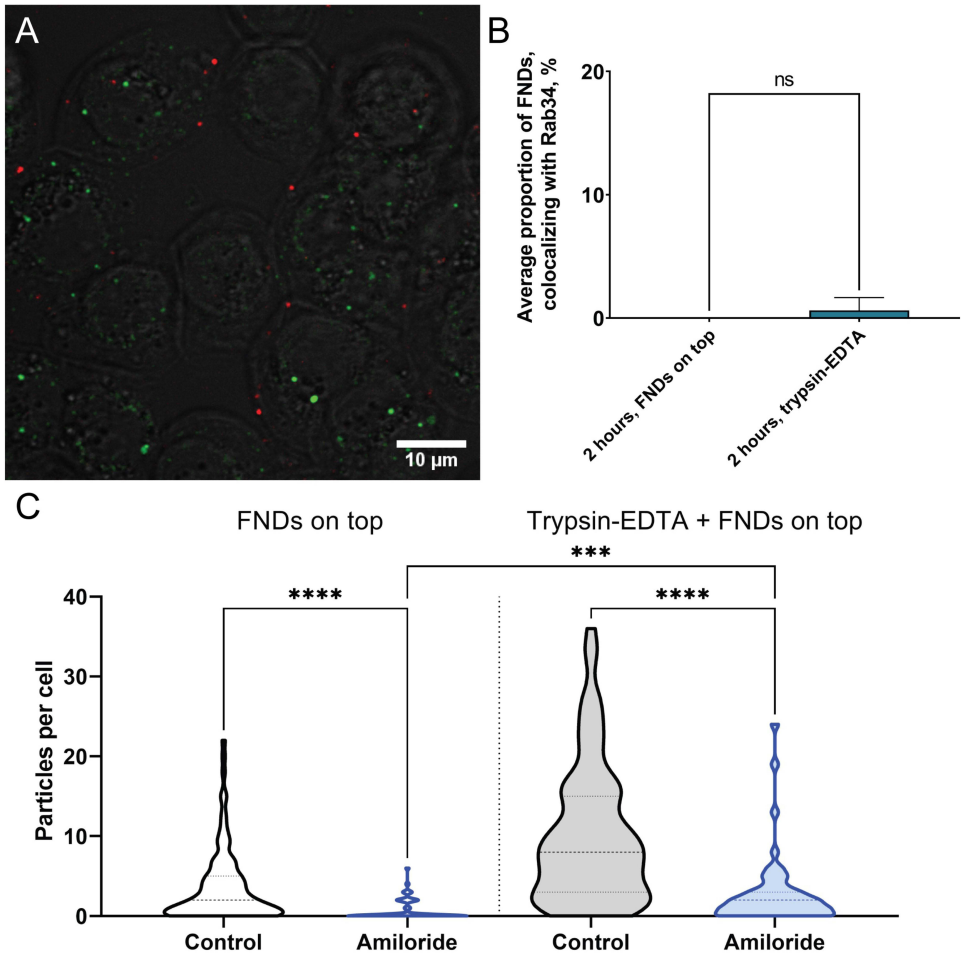

Figure 12 (**A**) HT-29 cells contain a relatively high number of large vesicles, positive for Rab34 (green), which is associated with macropinosomes. However, internalized FNDs (red) almost never colocalize with those (**B**), which indicates that macropinocytosis does not play a substantial role in the FND uptake in this cell line. (**C**) At the same time, amiloride significantly decreases the number of internalized FNDs in both control and trypsin-EDTA pre-treated cells. This effect is more pronounced in the control cells. Statistical significance of differences between the two control groups is not shown. Statistical differences are denoted by ns=not significant, ***p ≤ 0.001 and ****p ≤ 0.0001.

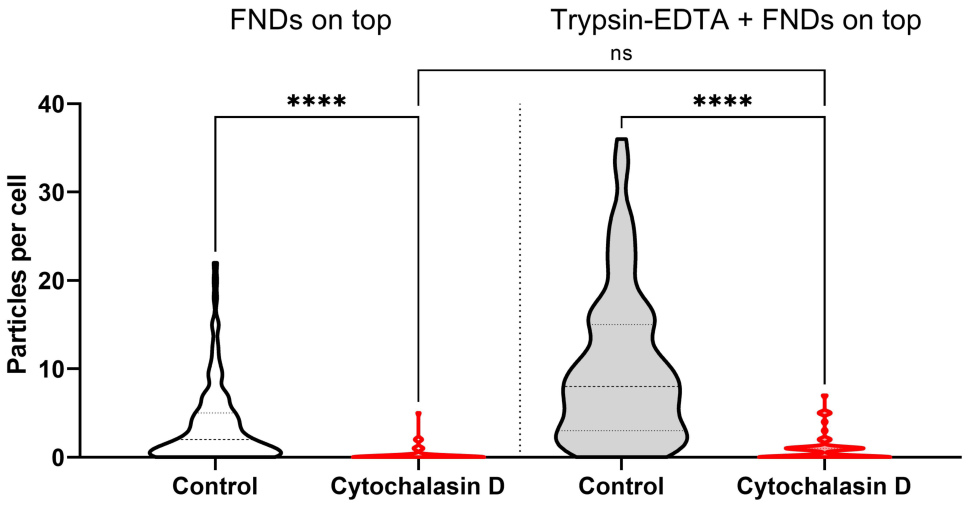

Figure 13 Number of internalized FNDs after (2+4) hours of incubation in presence of cytochalasin D. Statistical significance of differences between the two control groups is not shown. Statistical differences are denoted by ns=not significant and ****p ≤ 0.0001.

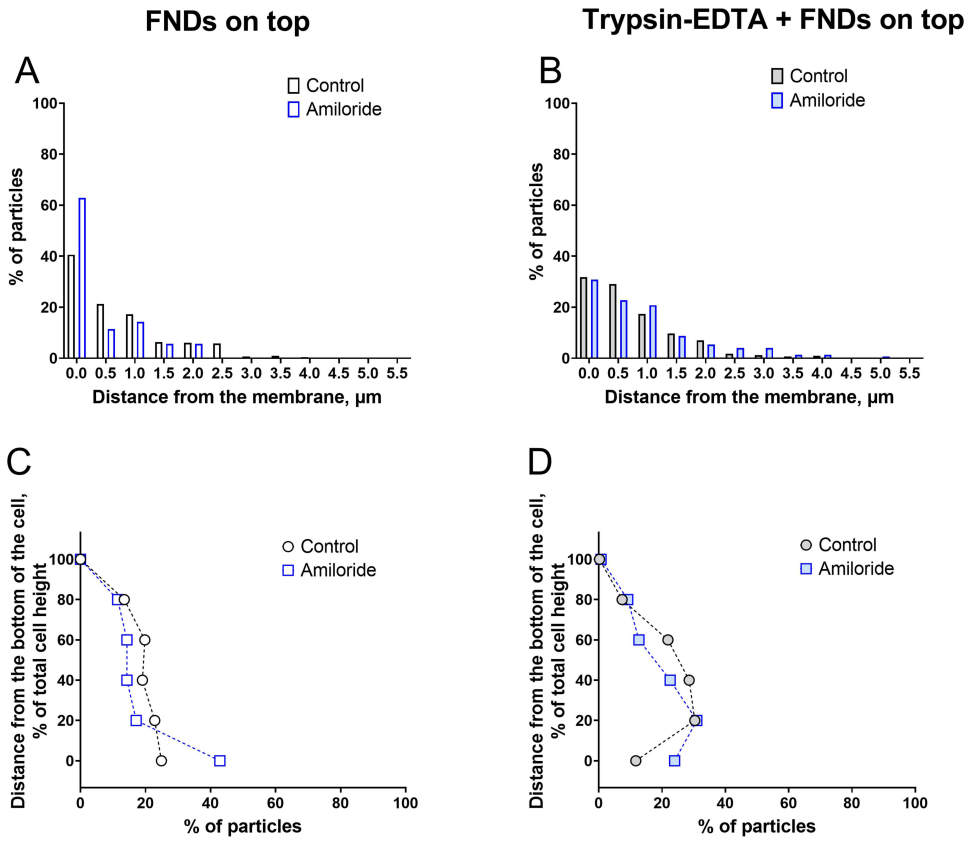

Figure 14 Intracellular distribution of internalized FNDs after (2+4) hours of incubation. Amiloride increases the proportion of particles at the cell membrane only in the control (**A**), but not in trypsin-EDTA-treated cells (**B**). It has similar effects on the vertical distribution of internalized FNDs in both experimental groups, increasing the proportion of particles at the very bottom of the cell and mildly decreasing the proportion of particles in the middle part of the cell (**C** and **D**).

interfere with actin dynamics, but its effects differ in various cell types. In vascular smooth muscle cells, for example, amiloride has been shown to induce hyperpolymerization of actin,[36] whereas renal epithelial cells respond with actin depolymerization.[35] The response of HT-29 cells has not been studied. However, a similar cell line, Caco-2, exhibits aggregates of polymerized actin, when treated with amiloride.[37] In line with this, cytochalasin D, a potent agent causing actin depolymerization, has the opposite effect on the trypsin-EDTA pre-treated and non-treated cells, which can be seen as circumstantial evidence of an actin-polymerizing effect of amiloride. More studies would, of course, be necessary to examine this hypothesis.

Interestingly, both amiloride and cytochalasin D exhibit their impact in the same vertical area of the cells – possibly acting on the same target. Some of the mechanisms, which have not been explored in this study, but are heavily dependent on actin polymerization, include glycosylphosphotidylinositol- anchored protein enriched compartments/clathrin-independent carriers (GEEC/CLIC) endocytosis (Figure 1) or flotillin-dependent endocytosis. Indeed, actin dynamics seem to play the central role in the clathrin- and dynamin-independent uptake pathways.[38] A number of these endocytic systems is also organized in a polarized manner in a cell, favoring the basolateral surface.[39] This possibility should be investigated as well, as this family of uptake mechanisms has been largely overlooked by the studies of nanodiamond-cell interactions.

To summarize, we show that nanodiamond internalization by the cells of epithelial origin is a complex and intricate process, which involves a number of mechanisms. Moreover, a simple and routine procedure, such as trypsin-EDTA treatment, commonly used in cell culture, can have profound impact on this process, changing not only the number of internalized FNDs, but the underlying pathways as well. Further, it is worth noting that treating

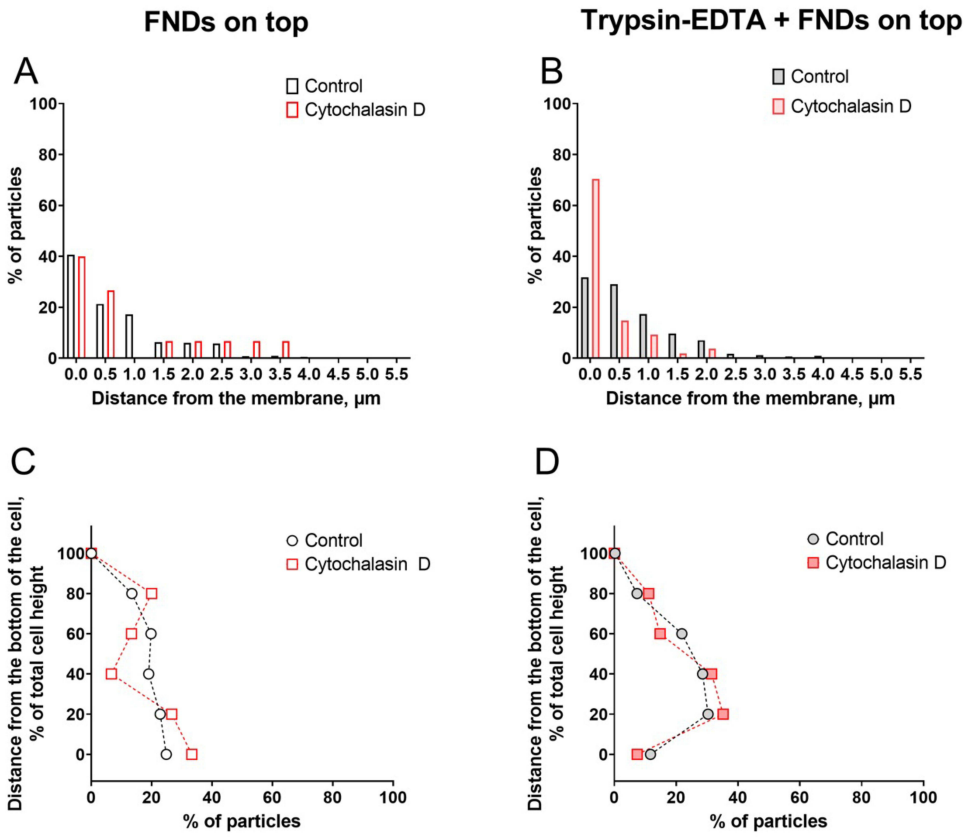

Figure 15 Intracellular distribution of internalized FNDs after (2+4) hours of incubation in presence of cytochalasin D. (**A**) Cytochalasin D barely affects the distance that FNDs travel away from the cell membrane in non-treated cells. (**B**) However, in trypsin-EDTA-treated cells, it leads to the accumulation of FNDs on the cell periphery. (**C**) In non-treated cells, cytochalasin D results in more FNDs present in the apical and the basal parts of the cell, as opposed to the middle region. (**D**) Its impact on the vertical distribution of FNDs in trypsin-EDTA-treated cells is far less pronounced.

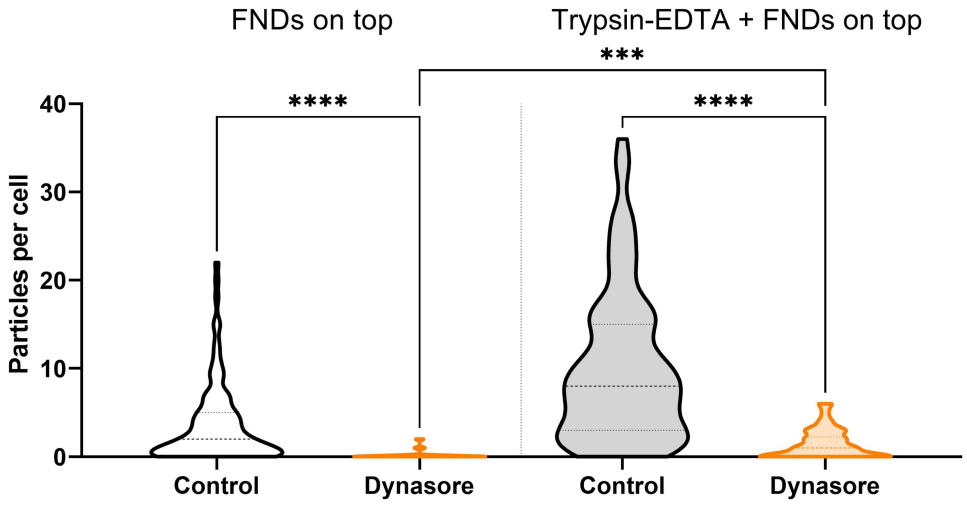

Figure 16 Number of internalized FNDs after (2+4) hours of incubation in presence of dynasore. Statistical significance of differences between the two control groups is not shown. Statistical differences are denoted by ***p ≤ 0.001 and ****p ≤ 0.0001.

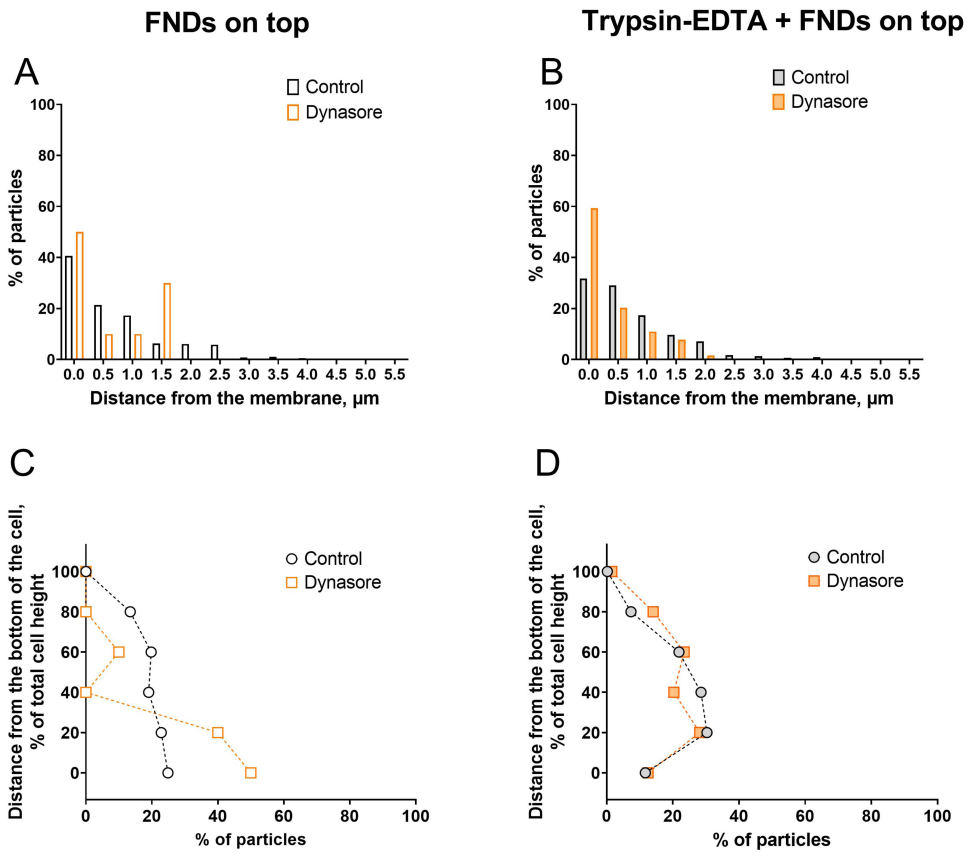

Figure 17 Intracellular distribution of internalized FNDs after (2+4) hours of incubation. Dynasore increases the proportion of particles at the cell membrane both in the control (**A**) and in trypsin-EDTA-treated cells (**B**). At the same time, in the "FNDs on top" group, treatment with dynasore causes another peak around 1.5 μm from the cell membrane. Notably, this is the farthest distance FNDs travel towards the centre of the cell. (**C**) Dynasore has similar effects on the vertical distribution of internalized FNDs to chlorpromazine: in non-treated cells, dynasore increases the proportion of particles at the basal part of the cell and decreases the apical population. (**D**) In the cells pre-treated with trypsin-EDTA, dynasore has a very mild effect on the vertical distribution of FNDs, causing slightly more FNDs to be in the apical part of the cell.

cells with trypsin-EDTA is impractical to use in vivo. However, there are several applications of nanodiamonds where this process can be applied. These applications include for instance mechanistic studies in cells with nanodiamonds[40–42] or ex vivo diagnostics.[43,44]

Table 3 Impact of Chemical Inhibitors on the Vertical Distribution of Internalized FNDs

Inhibitor	FNDs on Top		Trypsin-EDTA + FNDs on Top	
	Region of the Largest Decrease in FND Counts	Region of the Largest Increase in FND Counts	Region of the Largest Decrease in FND Counts	Region of the Largest Increase in FND Counts
Chlorpromazine	80% of total cell height (apical)	0% of total cell height (basal)	n/a	n/a
Genistein	0% of total cell height (basal)	100% of total cell height (apical)	40% of total cell height (middle)	20% of total cell height (basal)
Amiloride	60% of total cell height (middle)	0% of total cell height (basal)	60% of total cell height (middle)	0% of total cell height (basal)
Dynasore	40–80% of total cell height (middle, apical)	0% of total cell height (basal)	40% of total cell height (middle)	80% of total cell height (apical)
Cytochalasin D	40% of total cell height (middle)	0% of total cell height (basal)	60% of total cell height (middle)	20% of total cell height (basal)

Conclusions

In this study we analyze the uptake of nanodiamonds by HT-29 cells. While the uptake itself was reported earlier,[18] we here investigated the mechanism behind it. We show that nanodiamonds are internalized via a wide range of endocytic pathways, with clathrin-mediated endocytosis being the dominant one. Pre-treating the cells with trypsin-EDTA, even for a very short time, dramatically increases the number of internalized particles and affects the distribution of endocytic mechanisms involved in the uptake. Our findings emphasize the need to use complementary techniques to investigate the nanoparticle internalization pathways and highlight the complex nature of this process.

Data Sharing Statement

All data is available in this manuscript or on request from the corresponding author.

Acknowledgment

This paper is based on the thesis of Alina Sigaeva and Runrun Li. It has been published on the institutional website: https://research.rug.nl/en/publications/fluorescent-nanodiamonds-as-free-radical-sensors-in-live-mammalia

Funding

RS acknowledges financial support from the European Commission via an ERC starting grant (ERC-2016-STG Stress Imaging 714289). We would also thank the China Scholarships Council for supporting us with a scholarship and the de Cock Hadders Stichting for a grant for A. Sigaeva.

Disclosure

RS is founder of the spin off company QTsense who commercialise quantum sensing equipment. The activities of QTsense are not directly related to the work of this article. The authors report no other conflicts of interest in this work.

References

1. Weng MF, Chiang SY, Wang NS, Niu H. Fluorescent nanodiamonds for specifically targeted bioimaging: application to the interaction of transferrin with transferrin receptor. *Diamond Relat Mate.* 2009;18(2–3):587–591.
2. Brigger I, Dubernet C, Couvreur P. Nanoparticles in cancer therapy and diagnosis. *Adv Drug Delivery Rev* 2012;64:24–36. doi:10.1016/j.addr.2012.09.006
3. Sneider A, VanDyke D, Paliwal S, Rai P. Remotely triggered nano-theranostics for cancer applications. *Nanotheranostics*. 2017;1(1):1. doi:10.7150/ntno.17109
4. Marques Neto LM, Kipnis A, Junqueira-Kipnis AP. Role of metallic nanoparticles in vaccinology: implications for infectious disease vaccine development. *Front Immunol*. 2017;8:239. doi:10.3389/fimmu.2017.00239
5. van der Laan K, Hasani M, Zheng T, Schirhagl R. Nanodiamonds for in vivo applications. *Small*. 2018;14(19):1703838. doi:10.1002/smll.201703838
6. Liu GQ, Liu RB, Li Q. Nanothermometry with enhanced sensitivity and enlarged working range using diamond sensors. *Acc. Chem. Res.* 2023;56 (2):95–105. doi:10.1021/acs.accounts.2c00576
7. Chipaux M, van der Laan KJ, Hemelaar SR, Hasani M, Zheng T, Schirhagl R. Nanodiamonds and their applications in cells. *Small*. 2018;14 (24):1704263. doi:10.1002/smll.201704263
8. Zhang Y, Sharmin R, Sigaeva A, Klijn CW, Mzyk A, Schirhagl R. Not all cells are created equal–endosomal escape in fluorescent nanodiamonds in different cells. *Nanoscale*. 2021;13(31):13294–13300. doi:10.1039/D1NR02503A
9. Aderem A, Underhill DM. Mechanisms of phagocytosis in macrophages. *Ann Rev Immunol.* 1999;17(1):593–623. doi:10.1146/annurev.immunol.17.1.593
10. Sandvig K, Kavaliauskiene S, Skotland T. Clathrin-independent endocytosis: an increasing degree of complexity. *Histochemistry and Cell Biology*. 2018;150(2):107–118. doi:10.1007/s00418-018-1678-5
11. Mettlen M, Chen PH, Srinivasan S, Danuser G, Schmid SL. Regulation of clathrin-mediated endocytosis. *Annu. Rev. Biochem.* 2018;87 (1):871–896. doi:10.1146/annurev-biochem-062917-012644
12. Rejman J, Oberle V, Zuhorn IS, Hoekstra D. Size-dependent internalization of particles via the pathways of clathrin-and caveolae-mediated endocytosis. *Biochem. J*. 2004;377(1):159–169. doi:10.1042/bj20031253
13. Parton RG, Simons K. The multiple faces of caveolae. *Nat Rev Mol Cell Biol*. 2007;8(3):185–194. doi:10.1038/nrm2122
14. Wu M, Guo H, Liu L, Liu L. Size-dependent cellular uptake and localization profiles of silver nanoparticles. *Int j Nanomed*. 2019;14:4247. doi:10.2147/IJN.S201107
15. Liu D, Cheng B, Li D, Li J, Wu Q, Pan H. Investigations on the interactions between curcumin loaded vitamin E TPGS coated nanodiamond and Caco-2 cell monolayer. *Int J Pharm*. 2018;551(1–2):177–183. doi:10.1016/j.ijpharm.2018.09.030
16. Gilleron J, Querbes W, Zeigerer A, et al. Epstein-Barash. *Nature Biotechnol*. 2013;31(7):638–646. doi:10.1038/nbt.2612
17. Huang LH, Han J. Shape-dependent adhesion and endocytosis of hydroxyapatite nanoparticles on A7R5 aortic smooth muscle cells. *J Cell Physiol*. 2020;235(1):465–479. doi:10.1002/jcp.28987
18. Dutta D, Donaldson JG. Search for inhibitors of endocytosis: intended specificity and unintended consequences. *Cellular Logistics*. 2012;2 (4):203–208. doi:10.4161/cl.23967

19. Rennick JJ, Johnston AP, Parton RG. Key principles and methods for studying the endocytosis of biological and nanoparticle therapeutics. *Nature Nanotechnol*. 2021;16(3):266–276. doi:10.1038/s41565-021-00858-8
20. Sigaeva A, Morita A, Hemelaar SR, Schirhagl R. Nanodiamond uptake in colon cancer cells: the influence of direction and trypsin-EDTA treatment. *Nanoscale*. 2019;11(37):17357–17367. doi:10.1039/C9NR04228H
21. Moscariello P, Raabe M, Liu W, et al. Unraveling In Vivo Brain Transport of Protein-Coated Fluorescent Nanodiamonds. *Small*. 2019;15(42):1902992. doi:10.1002/smll.201902992
22. Krupa A, Descamps M, Willart JF, et al. High-energy ball milling as green process to vitrify tadalafil and improve bioavailability. *Mol Pharmaceut*. 2016;13(11):3891–3902. doi:10.1021/acs.molpharmaceut.6b00688
23 Solarska-Ściuk K, Gajewska A, Glińska S, et al. Intracellular transport of nanodiamond particles in human endothelial and epithelial cells. *Chem. Biol. Interact*. 2014;219:90–100. doi:10.1016/j.cbi.2014.05.013
24 Schrand AM, Lin JB, Hens SC, Hussain SM. Temporal and mechanistic tracking of cellular uptake dynamics with novel surface fluorophore-bound nanodiamonds. *Nanoscale*. 2011;3(2):435–445. doi:10.1039/C0NR00408A
25. Faklaris O, Joshi V, Irinopoulou T, et al. Photoluminescent diamond nanoparticles for cell labeling: study of the uptake mechanism in mammalian cells. *ACS nano*. 2009;3(12):3955–3962. doi:10.1021/nn901014j
26. Vaijayanthimala V, Tzeng YK, Chang HC, Li CL. The biocompatibility of fluorescent nanodiamonds and their mechanism of cellular uptake. *Nanotechnology*. 2009;20(42):425103. doi:10.1088/0957-4484/20/42/425103
27. Liu KK, Wang CC, Cheng CL, Chao JI. Endocytic carboxylated nanodiamond for the labeling and tracking of cell division and differentiation in cancer and stem cells. *Biomaterials*. 2009;30(26):4249–4259. doi:10.1016/j.biomaterials.2009.04.056
28. Shenderova OA, Shames AI, Nunn NA, Torelli MD, Vlasov I, Zaitsev A. Synthesis, properties, and applications of fluorescent diamond particles. *J Vac Sci Technol B Nanotechnol Microelectron*. 2019;37(3):030802. doi:10.1116/1.5089898
29. Hemelaar R, de Boer P, Chipaux M, et al. Nanodiamonds as multi-purpose labels for microscopy. *Sci Rep*. 2017;7(1):720. doi:10.1038/s41598-017-00797-2
30. Hemelaar SR, Nagl A, Bigot F, et al. The interaction of fluorescent nanodiamond probes with cellular media. *Mikrochim Acta*. 2017;184(4):1001–1009. doi:10.1007/s00604-017-2086-6
31. Abbas ZS, Sulaiman GM, Jabir MS, et al. Galangin/β-cyclodextrin inclusion complex as a drug-delivery system for improved solubility and biocompatibility in breast cancer treatment. *Molecules*. 2022;27(14):4521. doi:10.3390/molecules27144521
32. Ibrahim AA, Kareem MM, Al-Noor TH, et al. Pt (II)-thiocarbohydrazone complex as cytotoxic agent and apoptosis inducer in Caov-3 and HT-29 Cells through the P53 and caspase-8 pathways. *Pharmaceuticals*. 2021;14(6):509. doi:10.3390/ph14060509
33. Kadhim RJ, Karsh EH, Taqi ZJ, Jabir MS. Biocompatibility of gold nanoparticles: in-vitro and In-vivo study. Materials Today. *Proceedings*. 2021;42:3041–3045.
34. Sasahara T, Yayama K, Tahara T, Onoe H, Okamoto H. Na+/H+ exchanger inhibitor augments hyperosmolarity-induced vasoconstriction by enhancing actin polymerization. *Vascular Pharmacology*. 2013;59(5–6):120–126. doi:10.1016/j.vph.2013.07.004
35. Watts BA, George T, Good DW. The basolateral NHE1 Na+/H+ exchanger regulates transepithelial HCO 3− absorption through actin cytoskeleton remodeling in renal thick ascending limb. *J Biol Chem*. 2005;280(12):11439–11447. doi:10.1074/jbc.M410719200
36. Zuhorn IS, Kalicharan D, Robillard GT, Hoekstra D. Adhesion receptors mediate efficient non-viral gene delivery. *Mol Ther*. 2007;15(5):946–953. doi:10.1038/mt.sj.6300139
37. Unno N, Menconi MJ, Fink MP. Nitric oxide-induced hyperpermeability of human intestinal epithelial monolayers is augmented by inhibition of the amiloride-sensitive Na+-H+ antiport: potential role of peroxynitrous acid. *Surgery*. 1997;122(2):485–492. doi:10.1016/S0039-6060(97)90042-8
38. Mayor S, Parton RG, Donaldson JG. Cold Spring Harbor perspectives in biology. *Cold Spring Harbor Perspectives in Biology*. 2014;6(6):a016758. doi:10.1101/cshperspect.a016758
39. Shafaq-Zadah M, Dransart E, Johannes L. Clathrin-independent endocytosis, retrograde trafficking, and cell polarity. *Curr. Opin. Cell Biol*. 2020;65:112–121. doi:10.1016/j.ceb.2020.05.009
40. Reyes-San-Martin C, Hamoh T, Zhang Y, et al. Nanoscale mri for selective labeling and localized free radical measurements in the acrosomes of single sperm cells. *ACS nano*. 2022;16(7):10701–10710. doi:10.1021/acsnano.2c02511
41. Lin N, van Zomeren K, van Veen T, et al. Quantum Sensing of Free Radicals in Primary Human Granulosa Cells with Nanoscale Resolution. *ACS Cent. Sci*. 2023;9(9):1784–1798. doi:10.1021/acscentsci.3c00747
42. Morita A, Nusantara AC, Myzk A. Detecting the metabolism of individual yeast mutant strain cells when aged, stressed or treated with antioxidants with diamond magnetometry. *Nano Today*. 2023;48:101704. doi:10.1016/j.nantod.2022.101704
43. Elías-Llumbet A, Tian Y, Reyes-San-Martin C, et al. Quantum Sensing for Real-Time Monitoring of Drug Efficacy in Synovial Fluid from Arthritis Patients. *Nano Lett*. 2023;23(18):8406–8410. doi:10.1021/acs.nanolett.3c01506
44. Nie L, Nusantara AC, Damle VG, et al. Quantum sensing of free radicals in primary human dendritic cells. *Nano Lett*. 2021;22(4):1818–1825. doi:10.1021/acs.nanolett.1c03021